Applied Catalysis B: Environment and Energy 375 (2025) 125432

Contents lists available at ScienceDirect

Applied Catalysis B: Environment and Energy

journal homepage: www.elsevier.com/locate/apcatb

A novel versatile platform as efficient deoxydehydration (DODH) catalysts: Keggin polyoxometalates

Alixandre Magerat [a,*], Sophie Hermans [b], Eric M. Gaigneaux [a]

[a] Université catholique de Louvain (UCLouvain), Institute of Condensed Matter and Nanosciences (IMCN), - Molecular Chemistry, Materials and Catalysis (MOST), Place Louis Pasteur, 1 – box 04.01.09, Louvain-la-Neuve, Belgium
[b] Université catholique de Louvain (UCLouvain), Institute of Condensed Matter and Nanosciences (IMCN), - Molecular Chemistry, Materials and Catalysis (MOST), Place Louis Pasteur, 1 – box 04.01.03 – 1348, Louvain-la-Neuve, Belgium

ARTICLE INFO

Keywords:
Deoxydehydration
DODH
Keggin
Phospho(dodeca)molybdate
Phospho(dodeca)tungstate
Rhenium
Substitution

ABSTRACT

Despite their high tunability and versatility, the use of Keggin polyoxometalates (POMs) as deoxydehydration (DODH) catalysts has never been fully exploited. To date, only one study reported a single catalytic test using $H_3PMo_{12}O_{40}$ ($HPMo_{12}$), as part of a broader screening of various Mo-based catalysts[1]. In this contribution, we report for the very first time the promising catalytic performances in DODH of 1,2-hexanediol (chosen as model substrate) of tetrabutylammonium phosphododecamolybdate ($TBAPMo_{12}$) (100 % conversion, 52 % selectivity). This Keggin salt was easily obtained by ion metathesis and precipitation of the commercially available $HPMo_{12}$ with TBABr. Additionally, we show that it is possible to boost the catalytic performances of $(TBA)_3PW_{12}O_{40}$ ($TBAPW_{12}$), which in its pristine form is not as performant (45 % conversion, 23 % selectivity) as its Mo counterpart. To do so, the monolacunary form of PW_{12} was synthesized ($(TBA)_4H_3PW_{11}O_{39}$ = $TBAHPW_{11}$) and then metalated with a Re precursor, yielding a very active (100 % conversion, 73 % selectivity) $(TBA)_4PW_{11}Re^{V}O_{40}$ ($TBAPW_{11}Re$) mixed-metal compound. $TBAPW_{11}Re$ was fully characterized by PXRD, IR, ^{31}P NMR, ICP-AES, UV–vis and elemental analysis and its catalytic nature was investigated together with $TBAPMo_{12}$. Cold filtration tests and recycling experiments revealed that it is their partial dissolution that leads to DODH-active species. IR and ^{31}P NMR data indicated that these active species are the dissolved PMo_{12} and $PW_{11}Re$ POMs themselves and not monometallic species.

1. Introduction

The inherent polyoxygenated and polymeric nature of biomass [2], typically under the form of complex polyhydroxylated polymers (e.g. cellulose and hemicellulose), is a significant hurdle in their transformation into commodity chemicals. While research is ongoing on the biomass depolymerization issue [3,4], parallel effort is being performed to reduce its high oxygen content in order to enable integration in today's chemical industry [5,6].

Catalytic deoxydehydration (DODH), which transforms vicinal diols into the corresponding alkenes with the help of a sacrificial reductant [7] (Fig. 1), is an interesting deoxygenation pathway as it offers access to valuable alkene intermediates from bio-derived molecules (e.g. 1, 3-butadiene from erythritol [8], 1,3,5-hexatriene from sorbitol [2] or muconic acid from mucic acid [9]).

DODH catalysts are generally based on high valent Re [10,11], Mo [12,13], V [14,15] or quite recently W [16]. These catalysts can either be simple (commercial) salts (e.g. NH_4ReO_4 [17] or $(NH_4)_6Mo_7O_{24}$ [1]) or more elaborated complexes (e.g. modified cyclopentadienyl ReO_3 [18], dioxovanadium(V) dipicolinate [14] or dioxomolybdenum with modified salen ligands [19]). Some can be truly heterogeneous and recyclable catalysts when supported [11,20] while others are single-use homogeneous catalysts. Among them, Re-based catalysts are by far the best ones in terms of conversion and especially selectivity. However, the scarcity of Re has pushed researchers to use more Earth-abundant metals instead, such as Mo and V [21,22]. By contrast, to our knowledge, the use of Keggin polyoxometalates (POMs) – usually applied for oxidation [23,24] or acid [25,26] catalysis – has never been fully explored (the only exception is a non-discussed single catalytic test on $H_3PMo_{12}O_{40}$ in wide Mo-containing catalysts screening study[1]) as DODH catalysts.

Keggin POMs are oxygen-metal clusters containing $[XM_{12}O_{40}]^{n-}$ heteropolyanions (HPAs), with X being an heteroatom (e.g. P, Si or B)

* Corresponding author.
E-mail address: alixandre.magerat@uclouvain.be (A. Magerat).

https://doi.org/10.1016/j.apcatb.2025.125432
Received 17 February 2025; Received in revised form 13 April 2025; Accepted 2 May 2025
Available online 4 May 2025

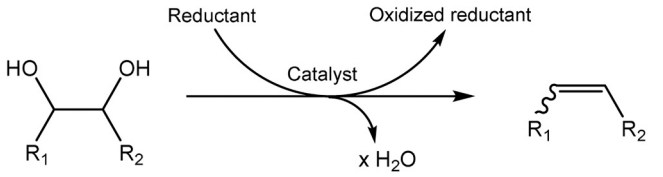

Fig. 1. Catalytic deoxydehydration. Depending on the nature of the reductant, x = 1 or 2.

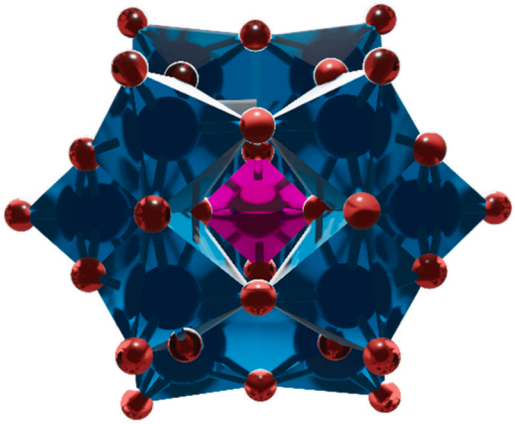

Fig. 2. Keggin heteropolyanion structure. Pink: heteroatom tetrahedron (XO_4). Blue: addenda metal octahedra (MO_6). Red: oxygen atoms. The counter-cations have been omitted for clarity.

and M being the addenda metal (often Mo^{VI} or W^{VI}) [26] (Fig. 2). A large variety of cations can counterbalance the negative charge of such complexes, such as H^+ [27], NH_4^+ [25] or K^+ [28], enabling to tune their acidity, hydrophobicity as well as their solubility in various organic solvents and water [24,25]. Alternatively, their chemical behavior can also be tailored by substituting one (or in some cases more [29]) addenda metal(s) by another transition metal (M'), yielding $[XM_{12-x}M'_xO_{40}]^{m-}$ mixed-metal anions. These possible chemical changes (use of different cations or addenda metal(s)) are generally carried out under green conditions (often not more than 80°C, in H_2O or acetonitrile and under air atmosphere) in comparison to the drastic conditions used for organometallic complexes syntheses, and provide Keggin POMs high tunability and versatility. This is why we initiated a study on their use as DODH catalysts.

In this contribution, we report and compare the catalytic performance of different Keggin phosphometalates with different cations and addenda metals in the model DODH reaction of 1,2-hexanediol into hexene. Additionally, the catalytically-active nature of some specific species is investigated.

2. Experimental section

2.1. Materials

1,2-hexanediol (98 %), phosphododecamolybdic acid hydrate, phosphododecatungstic acid hydrate, ammonium perrhenate (99 %), ammonium phosphododecamolybdate hydrate, chloroform and n-hexane were purchased from Sigma-Aldrich. Tetrabutyl ammonium bromide (>98 %) was purchased from Fluka. Hydrochloric acid (fuming, 37 % wt.), deuterated phosphoric acid in D_2O (85 %, 99 %D atom), deuterated acetonitrile (100 %D atom), dichloromethane and methanol were purchased from Carl Roth. 3-octanol (>98 %), 1,4-anhydroerythritol (>98 %) and 2,5-dihydrofuran (>98 %) were purchased from Tokyo Chemical Industry (TCI). $CDCl_3$ (99.80 % D) was purchased from Eurisotop. Unless otherwise indicated, all commercial compounds were used as received.

2.2. Synthesis of tetrabutylammonium phosphometalate ($(TBA)_3PM_{12}O_{40}$, M = Mo or W)

To a 250 mL erlenmeyer containing 15 mL of a freshly prepared 0.055 mol·L^{-1} $H_3PM_{12}O_{40}$ aqueous solution, 100 mL of a 0.03 mol·L^{-1} TBABr solution is added dropwise. A yellow (M = Mo) or white (M = W) precipitate formed immediately. The suspension was stirred overnight. The solid was recovered by vacuum filtration on a nylon filter (pore size = 0.22 µm), washed with distilled water and then dried overnight at room temperature under vacuum (<20 mbar).

2.3. Synthesis of ammonium phosphotungstate ($(NH_4)_3PW_{12}O_{40}$)

Ammonium phosphododecatungstate was synthesized according to the protocol described by Lang et al. [25] (see also supporting information). Essentially, the procedure is the same as described above, except that NH_4HCO_3 was used (instead of TBABr) to precipitate the solid from the $H_3PW_{12}O_{40}$ solution.

2.4. Synthesis of a Re-substituted phosphotungstate

2.4.1. Synthesis of tetrabutylammonium perrhenate ($TBAReO_4$)

In a 50 mL beaker, ammonium perrhenate (NH_4ReO_4, 200 mg) was dissolved in 15 mL distilled water. Then, 15 mL of an aqueous solution containing 400 mg tetrabutylammonium bromide (TBABr) was added. A white precipitate appeared immediately. The suspension was stirred overnight. The solid, that proved to be tetrabutylammonium perrhenate ($TBAReO_4$, see IR spectrum in Figure S0), was recovered by vacuum filtration on a nylon filter (pore size = 0.22 µm), washed with distilled water (3 × 100 mL) and then dried overnight at room temperature under vacuum (<20 mbar).

2.4.2. Synthesis of tetrabutylammonium tetrachlorooxorhenate(V) ($TBAReOCl_4$)

$TBAReOCl_4$ was synthesized according to the procedure described by Dilworth *et al.* [30]. All manipulations were carried under dry Ar atmosphere on a Schlenk line. $TBAReO_4$ (830 mg) was dissolved in $CHCl_3$ (6 mL) at 0°C (ice water bath). Me_3SiCl (5 mL) was then added dropwise, followed by the addition of dry deoxygenated MeOH (1.6 mL). The mixture was stirred for 3 h. Then, the volume was reduced (to approximately 2 mL) before adding a solution containing 10 mL EtOH and 10 mL Me_3SiCl. The solution was mixed vigorously and then placed at −33°C overnight. The formed yellow crystals were filtered out and washed three times with 30 mL dry cold (0°C) deoxygenated (by freeze-thaw cycles) n-hexane. The crystals were stored in a glovebox under Ar atmosphere.

2.4.3. Synthesis of tetrabutylammonium 11-tungstophosphate ($(TBA)_4H_3PW_{11}O_{39}$)

$H_3PW_{12}O_{40}{\cdot}nH_2O$ was dried under vacuum (<20 mbar) at 25°C overnight to obtain $H_3PW_{12}O_{40}{\cdot}6H_2O$ [26]. In a 250 mL beaker, 5 g of $H_3PW_{12}O_{40}{\cdot}6H_2O$ was dissolved in 30 mL of distilled water. Then, the pH (initially between 0 and 1) was adjusted between 5.0 and 5.5 with a NaOH (1 mol/L) aqueous solution. The pH-adjusted solution was then mixed with 25 mL distilled water containing 2.80 g TBABr. A white precipitate, that proved to be $(TBA)_4H_3PW_{11}O_{39}$ ($TBAHPW_{11}$), formed immediately. The solid was washed with distilled water (3 × 100 mL) and dried under vacuum (<20 mbar) at room temperature. ^{31}P NMR, FTIR, ICP-AES and elemental analysis were used to characterize the obtained product. Its ^{31}P NMR spectrum showed a single peak at δ = -11.89 ppm in CD_3CN (-11.91 ppm in literature [31]). Its FTIR spectrum (Fig. 4) presented two P-O asymmetric stretching peaks (1110 and 1053 cm^{-1}). ICP-AES (%wt) (calculated values): P 0.82 (0.85), W 55.41 (55.40). Elemental analysis (wt%) (calculated values): C 21.18 (21.06),

H 4.06 (4.06), N 1.49 (1.53) and O 17.15 (17.09).

2.4.4. Synthesis of tetrabutylammonium 11-tungstorheno(V)phosphate ($(TBA)_4PW_{11}Re^{V}O_{40}$)

$(TBA)_4PW_{11}Re^{V}O_{40}$ was synthesized according to the protocol described by Ortega *et al.* [32]. In a 50 mL round-bottom flask, 500 mg of $(TBA)_4H_3PW_{11}O_{39}$ was dissolved in 15 mL acetonitrile. Then, 110 mg of $TBAReOCl_4$ was added and the solution was stirred overnight. The solvent was evaporated with a rotary evaporator (40°C, 280 rpm). The dark purple solid was then recovered, washed with MeOH and recrystallized in acetone. ^{31}P NMR was used to characterize the obtained product. Its ^{31}P NMR spectrum showed a single peak at $\delta = -14.56$ ppm in CD_3CN. ICP-AES (%wt) (calculated values): P 0.76 (0.80), W 52.56 (52.54) and Re 4.81 (4.84). Elemental analysis (wt%) (calculated values): C 20.15 (19.97), H 3.76 (3.77), N 1.43 (1.46) and O 16.68 (16.62).

2.5. Impregnation of $TBAReO_4$ on $(TBA)_4H_3PW_{11}O_{39}$

In a 250 mL round-bottom flask, 500 mg of $(TBA)_4H_3PW_{11}O_{39}$ is suspended into 100 mL dichloromethane. Then, 20 mL of dichloromethane containing 90 mg of dissolved $TBAReO_4$ is added. The mixture is stirred 2 h before evaporating the solvent under reduced pressure at room temperature. The powder is recovered and further dried at < 20 mbar and 25°C overnight.

2.6. Catalytic tests

In a 15 mL closed pressure tube (LaborXing) equipped with a PTFE stir bar, 5 mL of a 3-octanol solution containing 0.5 mmol of 1,2-hexanediol (or 1,4-anhydroerythritol) and 0.5 mmol dodecane (internal standard), were added together with the solid catalyst (5 % mol Mo or W or 2 % Re with respect to 1,2-hexanediol). The tube was sealed with a PTFE screw cap and kept at the desired temperature (that ranged from 170°C to 220°C) in an oil bath. To stop the catalytic test, the tube was cooled down in an ice-cold water bath. Reactants and products were then quantified with a GC-2010 Plus equipped with a FID-2010 Plus detector, a SH-RTX-5 (30 m length, 0.25 mm inner diameter, 0.1 μm film thickness) column, an AOC-20s auto-sampler and an AOC-20i auto-injector from Shimadzu. A vial was filled with the reaction medium supernatant, obtained by filtrating it through a 0.22 μm pore size syringe-filter. An aliquot of 1 μL of the prepared vial was injected (injector temperature: 275°C, 70°C during 6 min and then 20 °C/min until 100°C. Gas flow: 30 mL/min He, 40 mL/min H_2 and 400 mL/min dry air. FID temperature: 270°C) and the analysis was performed in split mode (split = 15, inlet pressure = 25 psi).

Conversion, selectivity and yield were calculated by using the following equations:

$$Conversion(\%) = \frac{C_{diol}(t_0) - C_{diol}(t^*)}{C_{diol}(t_0)} \cdot 100$$

$$Selectivity(\%) = \frac{C_{alkene}(t^*)}{C_{diol}(t_0) - C_{diol}(t^*)} \cdot 100$$

$$Yield(\%) = \frac{C_{alkene}(t^*)}{C_{diol}(t_0)} \cdot 100 = Selectivity \cdot Conversion$$

Where C represents the molar concentration either of 1,2-hexanediol (or 1,4-anhydroerythritol) or of hexenes (1-hexene and its isomers, 2- and 3-hexene) (or 2,5-dihydrofuran). t_0 and t * correspond to the times at which the reactor is dipped into the oil bath (t_0) or the ice-cold water bath (t *).

2.7. Cold filtration tests

To explore whether leaching of DODH active species occurred, a catalytic test was started as described above and quenched in the kinetic regime (conversion not exceeding 40 %) by dipping the reactor in an ice-water bath. The solid was removed from the reaction medium by filtration (using a 0.2 μm pore size syringe filter) and the liquid fraction was put again in the same reaction conditions as before being quenched. Conversion and selectivity evolutions were monitored by GC to see whether they still increased or remained constant after removal of the solid.

2.8. Recycling tests

At the end of a catalytic test, the reactor was cooled down in an ice-water bath and the reaction mixture was transferred into a 1.5 mL Eppendorf tube. The mixture was centrifugated in a VWR MiniStar blueline microcentrifuge at 2000 g during about 1 min. The recovered solid was washed with n-hexane and then dried overnight at 25°C under vacuum (<20 mbar) before being reused as a catalyst, as described above.

3. Characterizations

3.1. Infrared spectroscopy

All spectra were recorded on a Bruker Equinox 55 equipped with a dielectric DTGS detector with an iris aperture of 5000 μm. One hundred scans were recorded with a spectral resolution of 4 cm^{-1} in the range 400–4000 cm^{-1}. For FTIR measurements, powders were diluted in dry KBr and pressed into self-supported wafers. A pure KBr wafer was also analyzed and used as background. For ATR measurements, powders were deposited and slightly pressed against a diamond crystal before recording their IR spectrum. Air was used as background each time. For liquid samples, a droplet was deposited between 2 NaCl wafers. The two NaCl wafers served as background.

3.2. Nuclear magnetic resonance (^{31}P and ^{1}H NMR)

Powders/Liquids were dissolved/mixed in about 0.5 mL CD_3CN or $CDCl_3$ in an NMR tube. A home-made capillary tube containing a D_3PO_4 85 % wt. aqueous (D_2O) solution was inserted in the tube as reference for ^{31}P NMR experiments. All samples presented a peak at −12.45 ppm for ^{31}P NMR experiments due to a contamination present in the capillary. The analyses were performed on a Bruker Advance II spectrometer (Larmor frequency of 400 MHz for ^{1}H) or on a Jeol JNM-ECZL G series spectrometer (Larmor frequency of 600 MHz for ^{1}H), as the first spectrometer was replaced by the second one during the course of this study. The ^{31}P NMR spectra were recorded at room temperature, collecting 1064 scans with a relaxation delay of 2 s and a spectral width of 200 ppm. The ^{1}H NMR spectra were recorded at room temperature, collecting 32 scans with a relaxation delay of 2 s and a spectral width of 14 ppm.

3.3. Ultraviolet-visible spectroscopy (UV–vis)

Solutions were analysed on a Shimadzu UV-3600 Plus Series spectrometer in quartz High Precision Cells from Hellma Analytics. The spectra were recorded from 200 nm to 800 nm with a 0.5 nm sampling interval (slit width of 2 nm). From 200–380 nm, a deuterium lamp from Shimadzu was used as source while a W halogen lamp was used as source for the rest of the spectrum.

3.4. Powder X-ray diffraction (PXRD)

Diffractograms of the powder samples were recorded on a Bruker-D8

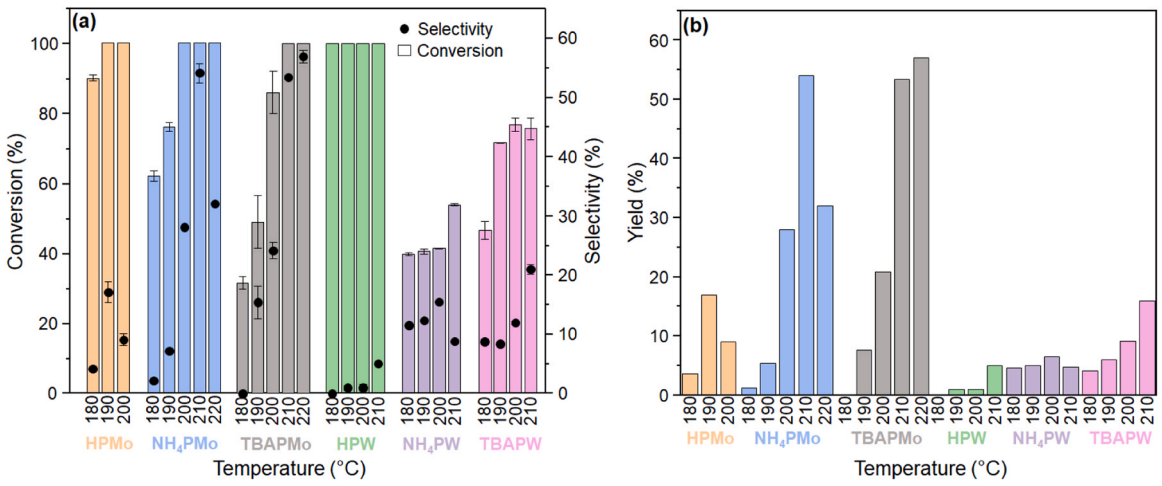

Fig. 3. Catalytic results (conversion of 1,2-hexanediol, selectivity and yields for hexene) with different phosphododecamolybdates and phosphododecatungstates at different reaction temperatures and with different counter-cations (H^+, NH_4^+ and TBA^+). Reaction conditions: 5 mL of a solution containing 0.1 mol/L 1,2-hexanediol and 0.1 mol/L n-dodecane (internal standard), 5 % mol M (M= Mo or W), 18 h at a given temperature: (a) Conversion and selectivity (b) Yield.

Advance diffractometer with a Bragg-Brentano geometry. A copper anode (Kα = 0.1548 nm) operated under 40 kV and 30 mA was used as X-ray source. The detector was a LynxEye XE-T. The angle (2θ) was varied from 5° to 80° at a speed of 5.93°/min (5051 steps of 0.015°). Well-grinded powders were dispersed on a "zero noise" sample holder coated with Vaseline or Nivea creme before insertion in the apparatus.

3.5. Inductively coupled plasma-atomic emission spectroscopy and elemental analysis

The digestion of $TBAHPW_{11}$ and $TBAPW_{11}Re$ proceeded as follows. About 50 mg of the sample was introduced in a 50 mL polypropylene tube. Then, 6 mL H_2SO_4 (95 % wt.) was added together with 2 mL H_2O_2 (35 % wt). Afterwards, 1 mL HF (40 % wt) was added. The tube was gently mixed and then allowed to cool down to room temperature. Finally, 12 mL of a home-made saturated H_3BO_3 aqueous solution was added. This last step enables to use a quartz nozzle during the ICP-AES analysis while using HF for the digestion. The Varian Vista MPX CCD instrument was used to perform the ICP-AES analyses. The elemental analyses were performed on a Thermo Scientific FlashSmart elemental analyser directly on solid samples.

4. Results and discussion

Keggin phosphododecamolybdates ($PMo_{12}O_{40}^{3-}$ = PMo) and phosphododecatungstates ($PW_{12}O_{40}^{3-}$ = PW) were first considered as potential catalysts for the DODH reaction. Three different counter-cations were considered: H^+ (the acid form, HPM), NH_4^+ (the most common counter-cation, NH_4PM) and TBA^+ (bulkier cation, TBAPM), with M being Mo or W. As only the acid forms and NH_4PMo are available commercially, the three other species (NH_4PW, TBAPW and TBAPMo) were prepared by ion metathesis and precipitation. Their Keggin structure was confirmed by FTIR and PXRD (Figure S1 & S2) in all cases.

The PMo and PW species with different counter-cations (H^+, NH_4^+ and TBA^+) were then tested as catalysts in the 1,2-hexanediol DODH with 3-octanol as both reductant and solvent and at different reaction temperatures (Fig. 3).

Within each series, the acidic species HPMs (M = Mo or W) showed the highest conversion but low selectivity due to their very high Bronsted acidity [26] which is reported in the literature to promote

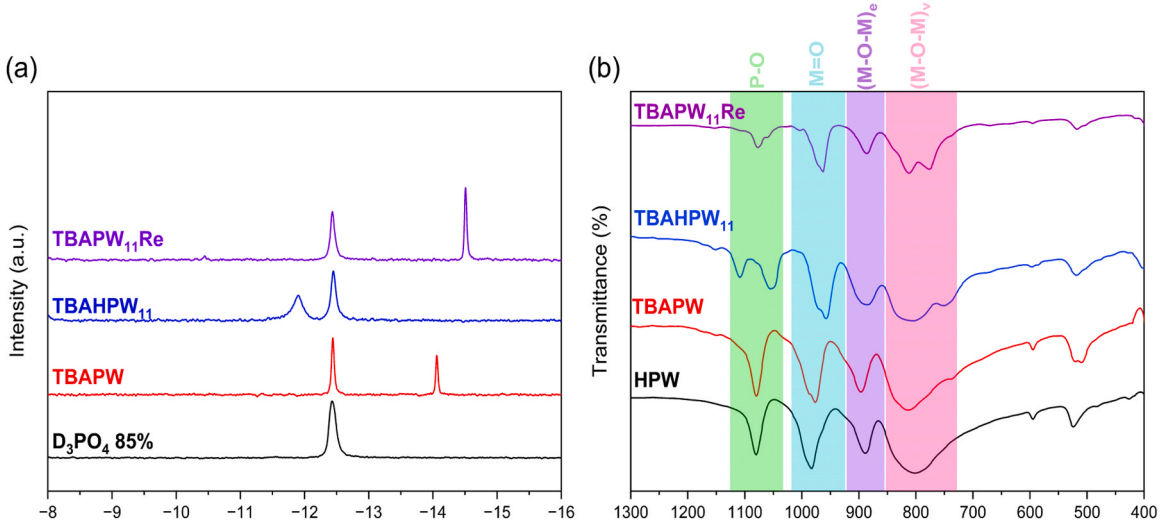

Fig 4. (a) ^{31}P NMR spectra of TBAPW, $TBAHPW_{11}$ and $TBAPW_{11}Re$. D_3PO_4 is plotted as reference (Note: it presents a contamination peak at −12.45 ppm from the capillary tube used for these analyses). (b) IR spectra of HPW, TBAPW, $TBAHPW_{11}$ and $TBAPW_{11}Re$. HPW is plotted for comparison. M = Re or W. The full IR spectra are available in Fig. S4.

side-reactions (e.g. acetalization [33]). For both the Mo- and W-based series, the hexene yield (Fig. 3(b)) was the best when using TBA^+ as counter-cation. Within the Mo-series, hexene isomers (2- or 3-hexene) were only observed with NH_4PMo and HPMo as catalysts while TBAPMo yielded only 1-hexene (Figure S3). These results are in line with the fact that acidity is well-known to promote isomerization of alkenes [34,35]. Hence, TBAPMo being not acidic, only 1-hexene was produced. TBAPMs showed higher yields than their NH_4PM counterparts, likely because the ammonium cation still presents some Bronsted acidity [25] as opposed to TBA^+.

For all the tests, the conversion increased with temperature (until a maximum of 100 %). This can be explained by the Arrhenius law and by considering a system in which the different chemical equilibria involved are not thermodynamically limited, which is here the case [7,33].

Besides, PW demonstrated lower DODH-activity than their PMo counterparts. The origin of this difference likely lies within the redox properties of W, especially its lower reducibility compared to Mo [16]. Phosphododecamolybdates have indeed reduction potentials about 400 mV higher than phosphododecatungstates [36,37], which gives them more redox flexibility. One way to tune the redox properties of Keggin HPAs, hence to overcome the lack of reducibility of W, is to replace one addenda metal by another one. We therefore consented to a synthetic effort to replace one of the twelve tungsten atoms of the PW anion with a high-valent Re(V) atom, as Re is a metal known to be very efficient at catalyzing DODH mainly under the form of organometallic complexes [10].

To do so, HPW was dissolved in distilled water (pH = 0–1) and the pH was subsequently increased (5.0 <pH<5.5) with a NaOH solution to yield the monolacunary form of PW, namely $PW_{11}O_{39}^{7-}$. This species was precipitated from its solution by adding TBABr, yielding $(TBA)_4H_3PW_{11}O_{39}$ (in short $TBAHPW_{11}$). $TBAHPW_{11}$ was then redissolved in acetonitrile and mixed with a home-made synthesized rhenium precursor ($TBAReOCl_4$) to refill the lacuna. The purified final product, $(TBA)_4PW_{11}Re^{V}O_{40}$ ($TBAPW_{11}Re$ in short), was characterized by ^{31}P NMR, UV–vis and FTIR as well as ICP-AES, elemental analysis (see experimental section) and PXRD (Figure S4 [38]).

^{31}P NMR indicated that the synthesis yielded pure $TBAPW_{11}Re$, with no other phosphorus-containing impurities (Fig 4 (a)) while ICP-AES and elemental analyses confirmed the $TBAPW_{11}Re$ stoichiometry (see experimental section). The chemical shift observed for $TBAPW_{11}Re$ in ^{31}P NMR (-14.56 ppm) is in excellent agreement with the values reported in literature (-14.93, −15.1 and −14.59 ppm for $(Me_2NH_2)_4PW_{11}ReO_{40}$ in DMSO-d_6, $K_4PW_{11}ReO_{40}$ in D_2O and $TBA_4PW_{11}ReO_{40}$ in CD_3CN, respectively) [39–42]. The Keggin structure was preserved as well, as shown in Fig. 4 (b) (Full IR spectra in Figure S5). Indeed, 4 characteristic peaks of the Keggin structure can be observed in the IR spectrum of $TBAPW_{11}Re$. Peaks at 1082 cm^{-1} and 981 cm^{-1} are attributed to the asymmetric stretching vibration of P-O and M=O (M=W or Re), respectively. The bands at 894 cm^{-1} and 818 cm^{-1} are attributed to asymmetric stretching vibrations of M-O-M (M=Re or W) (edge-shared oxygen) and M-O-M (vertex-shared oxygen), respectively. The IR spectrum of $TBAHPW_{11}$ exhibited two distinct peaks (instead of one) in the region attributed to P-O asymmetric stretching. This band splitting (going from the saturated TBAPW to the monolacunary one $TBAPHW_{11}$) is explained by an important symmetry decrease in the PW anion owing to the created vacancy [43]. On the contrary, $TBAPW_{11}Re$ and TBAPW presented very similar IR spectra. This was attributed (1) to the fact that the W vacancy was replenished when $TBAPHW_{11}$ was put in the presence of the Re precursor ($TBAReOCl_4$), thus rebuilding a symmetry of the anion very close to the one of TBAPW with consequently the P-O asymmetric stretching band not being split anymore, and (2) to the similar masses of W (183.8 amu) and Re (186.2 amu) [29]. Still, one could observe a small shoulder appearing on the P-O band of $TBAPW_{11}Re$. This can be explained by the substitution of W^{VI} by the smaller Re^{V} cation [41]. This band shouldering is more easily discernible in Fig. 8(b), as this spectrum has been taken in the transmission mode.

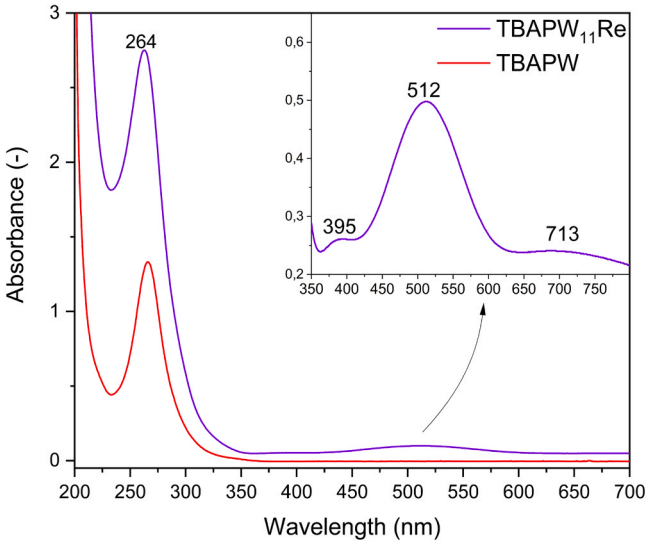

Fig. 5. UV–vis spectra of $(TBA)_4PW_{11}ReO_{40}$ and $(TBA)_3PW_{12}O_{40}$ dissolved in acetonitrile. The inset contains a zoom in the 350–800 nm region of a more concentrated $TBAPW_{11}Re$ solution.

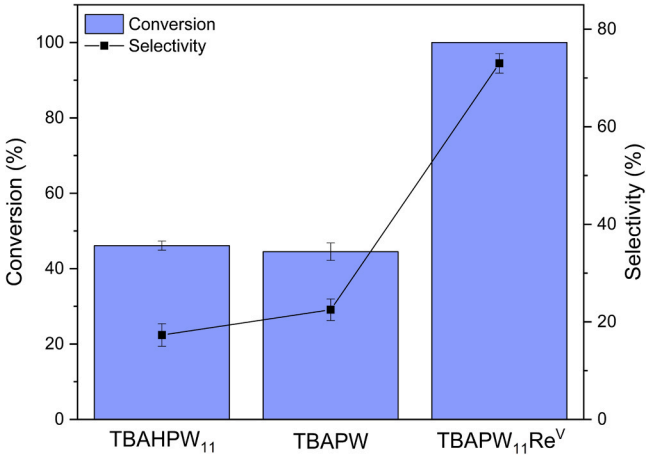

Fig. 6. Catalytic results (selectivity is for 1-hexene) with $(TBA)_4H_3PW_{11}O_{39}$ ($TBAHPW_{11}$), $(TBA)_3PW_{12}O_{40}$ (TBAPW) and $(TBA)_4PW_{11}Re^{V}O_{40}$ ($TBAPW_{11}Re$). Reaction conditions: 10 mg of solid and 5 mL of a solution containing 0.1 mol/L 1,2-hexanediol and 0.1 mol/L n-dodecane (internal standard), 18 h at 210°C.

Additionally, $TBAPW_{11}Re$ was dissolved in acetonitrile and its UV–vis spectrum was measured together with TBAPW for comparison (Fig. 5). Three additional peaks specific to the $PW_{11}ReO_{40}^{4-}$ anion were observed at 395, 512 and 713 nm [39,44]. These peaks are attributed to intervalence charge transfer transitions ($Re^{V} \rightarrow W^{VI}$) [39,44]. The molar extinction coefficients at 395, 512 and 713 nm aligned with the ones reported in literature [44]. Based on these coefficients, we estimated the purity of $TBAPW_{11}Re$ to be about 97 ± 2 % (see supporting information for detailed calculations).

$TBAPW_{11}Re$, $TBAHPW_{11}$ and TBAPW were tested and compared in terms of catalytic performances (Fig. 6). TBAPW and $TBAHPW_{11}$ converted 1,2-hexanediol into 1-hexene with the same yield (9 %). Substituting one W by one Re improved its catalytic performance tremendously. Indeed, $TBAPW_{11}Re$ showed much better catalytic performance than the pristine TBAPW, converting 1,2-hexanediol into 1-hexene with a yield of 73 %.

It should be noted that this strategy, *i.e.* substituting one Mo by one Re, could not be followed for PMo. This would have required indeed to first synthesize the monolacunary species of PMo, namely

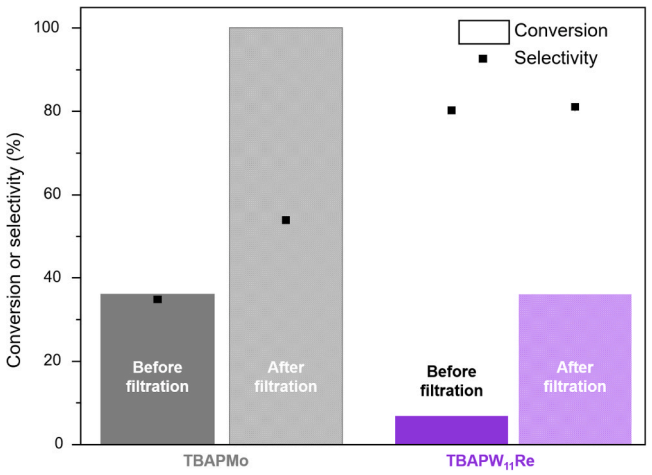

Fig. 7. Cold filtration tests of TBAPMo and TBAPW$_{11}$Re. The solid was filtrated after 7 h and 2 h of reaction for TBAPMo and TBAPW$_{11}$Re, respectively. The liquid was analyzed after 18 h or 7 h reaction for TBAPMo and TBAPW$_{11}$Re, respectively. Reaction conditions: 5 % mol. Mo or 2 % mol Re, 210°C.

$(TBA)_4H_3PMo_{11}O_{39}$ ($TBAHPMo_{11}$), and then to carry out the metalation by using $TBAReOCl_4$. However, this synthesis route cannot be envisaged as $ReOCl_4^-$ being a mild reductant, it would readily reduce $TBAHPMo_{11}$ into the one-electron reduced PMo [45], namely $PMo_{11}^{VI}Mo^{V}O_{40}^{4-}$, rather than having Re filling the Mo lacuna. As stated above, the fact that $TBAHPW_{11}$ can be metalated by $TBAReOCl_4$ (but not $TBAHPMo_{11}$) is actually possible thanks to its lower reducibility.

When performing the catalytic tests, it was observed that most of the TBAPMo and TBAPW$_{11}$Re species remained solid, which led us think that the catalysis was operating in a heterogeneous catalytic way. However, cold filtration tests indicated that some dissolved species were catalyzing the reaction. Indeed, the conversion continued increasing when the solids were filtered out of the reaction medium (Fig. 7). The solids were recovered, as partial re-precipitation of the dissolved species was likely to occur upon temperature decrease during the reaction quenching (from 210°C to 0°C). The remaining liquids after catalytic tests were recovered as well and their IR and UV–vis spectra were recorded (Figures S6 & S7). No conclusion could be drawn from the IR spectra as they were all identical, and the same as a reaction medium with no catalyst. No conclusion could be drawn either from UV–vis spectra, as the peaks could not be compared with literature data. The solids were also analyzed by IR to check the Keggin structure (Fig. 8). No difference could be observed before and after catalytic test for TBAPW$_{11}$Re while the two Mo-O-Mo bands broadened and the intensity of the Mo-O-Mo (edge-shared oxygen) decreased after catalyst test for TBAPMo. This change has already been reported for reduced phosphomolybdate species and is attributed to a strong coupling of bipolaron with the vibration of the bridging Mo-O-Mo bonds [46]. Still, these results are in line with a preserved Keggin structure. The reduction of TBAPMo was also inferred by its color change (from yellow-light green to dark blue) [47] during the reaction while TBAPW$_{11}$Re color remained the same (Figure S8). The reduction of TBAPMo was confirmed by UV–vis spectroscopy (Fig. 9), as the new band observed in its UV–vis spectrum corresponds to intervalence charge transfer transitions (IVCT) from Mo^{V} to Mo^{VI} [48]. The fact that Mo was dark blue at 100 % 1, 2-hexanediol conversion is not surprising as the catalytic tests were carried out with a very large excess of reductant (3-octanol being also the solvent of the reaction). In contrast, TBAPW$_{11}$Re presented the same UV–vis spectrum after the catalytic test than before (Fig. 5). This seems logical, as Re was already in a reduced oxidation state (+V) [44] when starting the reaction.

Accordingly, the ^{31}P NMR spectrum of TBAPW$_{11}$Re after catalytic test was the same as the fresh one, while the reduced TBAPMo indicated several new peaks (Fig. 10). All these new peaks are believed to be due to different reduced TBAPMo species [49] (namely $(TBA)_3PMo_{12-x}^{VI}Mo_x^{V}$). Some of the peaks seem to correspond to 4- and 6-electrons reduced TBAPMo species, by comparison with some published data [49]. Some other peaks differed from the literature data, probably because they related to reductions with other reductants. Additionally, the chemical shifts reported in literature were measured under different analysis conditions (e.g. use of different NMR solvents). The recovered powder after catalytic test was mixed with a large excess of Br_2 in order to reoxidize it. The obtained TBAPMo was green and its ^{31}P NMR spectrum showed one single peak at −2.54 ppm, demonstrating that the reduced state of TBAPMo is reversible. According to literature, this chemical shift could be attributed to $PMo_{12}O_{40}^{4-}$ or $P_2Mo_{18}O_{62}^{6-}$ (Wells-Dawson-like POMs) [45,50]. However, the latter possibility was discarded as the IR spectrum unequivocally showed a Keggin fingerprint. Indeed, in the case this reoxidation step would have generated $P_2Mo_{18}O_{62}^{6-}$, the IR spectrum would present two frankly distinguishable $(Mo\text{-}O\text{-}Mo)_{v \text{ or } e}$ peaks (instead of one for the Keggin) [51].

Cold filtration tests evidenced the presence of soluble DODH-active species (Fig. 7). However, solid particles of TBAPMo or TBAPW$_{11}$Re could be recovered at the end of the catalytic tests. We thus investigated whether the solid particles exhibited catalytic activity or if only the dissolved species were active. Assuming thermodynamic dissolution

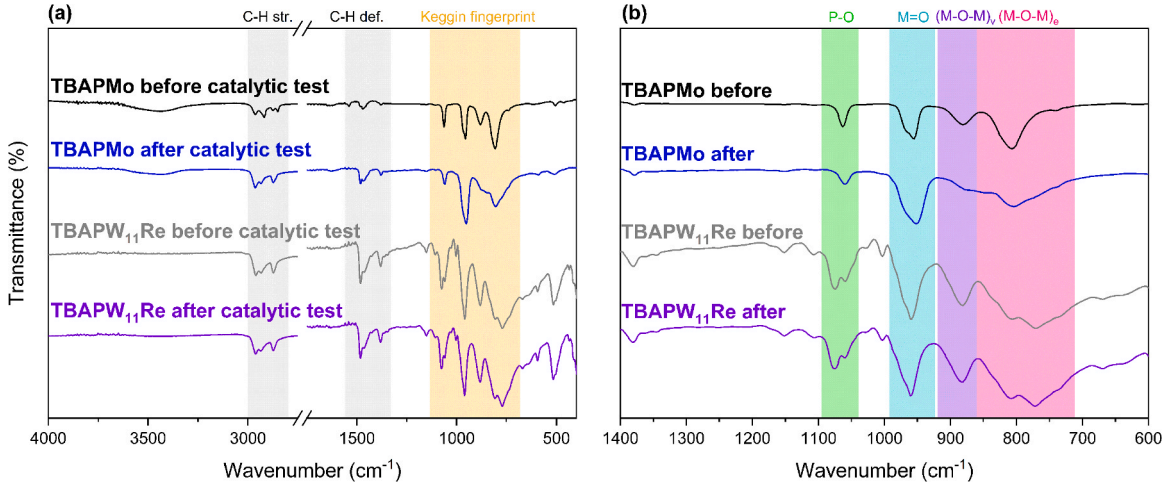

Fig. 8. IR spectra of TBAPMo and TBAPW$_{11}$Re before and after one catalytic test of 18 h at 210°C: (a) whole spectrum; (b) zoom on the Keggin fingerprint; M = Mo, W or Re.

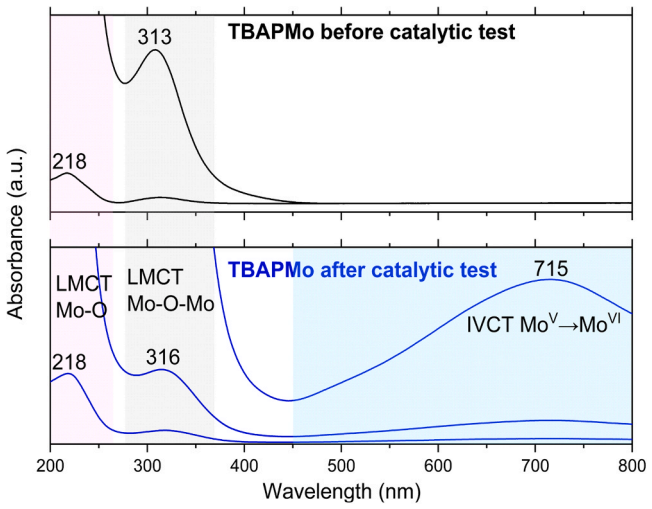

Fig. 9. UV–vis spectra of TBAPMo in CH_3CN before and after catalytic tests. As the absorption coefficients are not the same at each wavelength, solutions of different TBAPMo concentrations were measured (before and after catalytic test). The pink and the grey regions correspond to ligand to metal charge transfer transitions of Mo-O and Mo-O-Mo, respectively. Only TBAPMo after catalytic test presented a broad peak at 715 nm owing to Mo^{V} to Mo^{VI} transitions (blue highlighted region). Concentrations used (estimation): 47 and 2 μmol/L (before catalytic test) & 250, 38 and 6 μmol/L (after catalytic test).

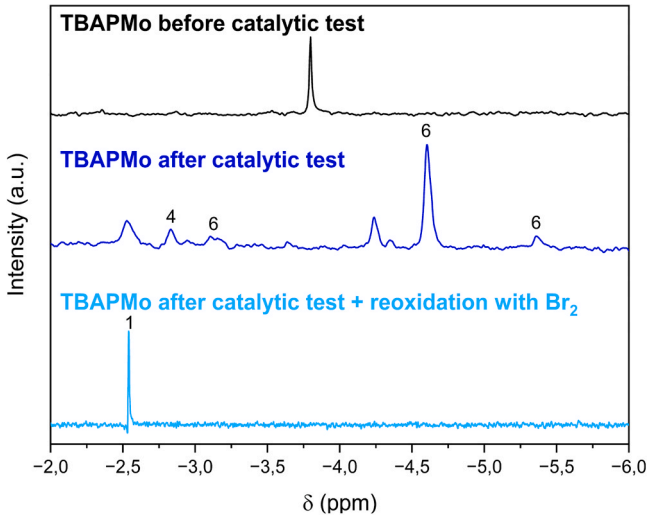

Fig. 10. ^{31}P NMR (in CD_3CN) spectra of TBAPMo before and after catalytic test (with and without reoxidation with Br_2). The numbers above the blue peaks are the number of electrons believed to have been involved in reducing the fresh TBAPMo to give the species responsible for these peaks.

equilibrium of TBAPMo and $TBAPW_{11}Re$ in the medium, the catalytic performance should remain constant as long as suspended solids are observed during catalytic testing. Under this hypothesis, we decided to reuse the solid particles of TBAPMo and $TBAPW_{11}Re$ (Fig. 11).

The recycled TBAPMo converted less 1,2-hexanediol (81 %) in comparison to the fresh one (100 %). This conversion decrease coincided with a translucent liquid mixture (no visible solid particles), meaning that it was no longer a saturated solution, hence explaining this lower conversion. $TBAPW_{11}Re$ showed a similar behavior. Its first reuse did not suffer any performance loss but the subsequent recycle gave lower conversion with no visible solid anymore. A similar trend was observed when recycling the catalysts at lower reaction time (hence not at full conversion) (Figures S9 and S10). These results suggest that solid

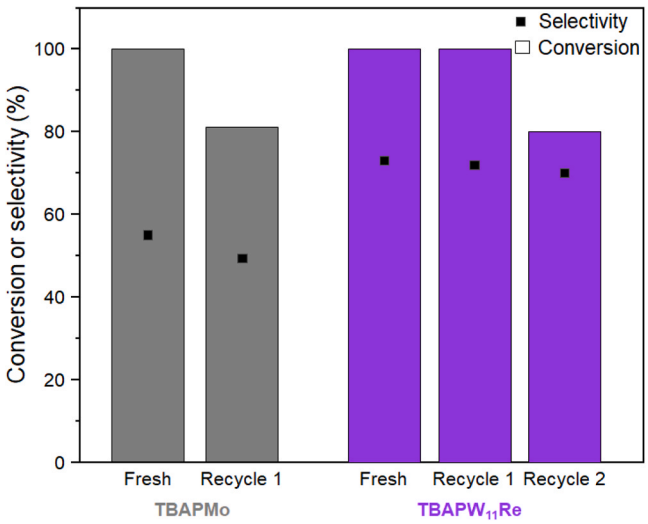

Fig. 11. Recycling experiments of TBAPMo and $TBAPW_{11}Re$. Reaction conditions: 18 h, 210°C, 0.1 mol/L 1,2-hexanediol and n-dodecane (internal standard) in 3-octanol (solvent), 2 %Re mol. and 5 %Mo mol.

TBAPMo and $TBAPW_{11}Re$ particles act as reservoirs for active species rather than catalysts themselves. Indeed, the conversion decrease was consistently observed alongside the continuous dissolution of TBAPMo or $TBAPW_{11}Re$ during the recycling experiments, likely due to a lower quantity of dissolved species compared to a saturated TBAPMo or $TBAPW_{11}Re$ solution in the case of recyclings.

The nature of these dissolved active species was then investigated. As stated above, the IR spectra of the liquid medium (recovered by filtering the reaction medium at 0°C at the end of catalytic tests performed with TBAPMo and $TBAPW_{11}Re$) were not useful. As the dissolved active species were suspected to precipitate during the reaction quenching (cooling from 210°C to 0°C), the reaction media were filtered at 90°C instead. Then, the supernatants were allowed to cool down at 4°C overnight. A precipitate was obtained in both cases and was analyzed by IR (Fig. 12). The IR spectrum of the solid recovered from the catalytic test with TBAPMo was very similar to reduced TBAPMo, as expected (Fig. 12 (a)). The $(Mo\text{-}O\text{-}Mo)_v$ band was not observable anymore and the $(Mo\text{-}O\text{-}Mo)_e$ was broader. As stated above, these changes have already been reported with reduced $PMo^{VI}_{12-x}Mo^{V}_{x}O_{40}^{(x+3)-}$ species [52–54] and are attributed to a strong coupling of bipolaron with the vibration of the bridging Mo-O-Mo bonds [46]. In the case of $TBAPW_{11}Re$, no difference could be observed between the solid recovered and the freshly synthesized $TBAPW_{11}Re$ (Fig. 12 (b)).

These results indicate that the Keggin structure of TBAPMo and $TBAPW_{11}Re$ is preserved all along the dissolution and the reprecipitation process during the catalytic tests. In other words, it seems that intact PMo and $PW_{11}Re$ polyoxometalates are the active species. However, these results cannot exclude a mechanism where the Keggin POM is temporarily unbundled in solution to operate catalytically as monomeric species, before reforming itself. Although this event seems quite unlikely, some experimental data demonstrating that this hypothesis can be discarded are exposed hereunder.

In the case of $TBAPW_{11}Re$, literature reports that its stability depends on the oxidation state of Re [32,44]. Pentavalent and hexavalent Re ($TBAPW_{11}Re^{V}$ and $TBAPW_{11}Re^{VI}$, respectively) are reported to be stable while the heptavalent one ($TBAPW_{11}Re^{VII}$) is hydrolyzed into ReO_4^- in water-containing media [44]. Literature generally reports DODH mechanisms with Re^{V}/Re^{VII} or Re^{IV}/Re^{VI} cycles [6,11,55]. In the case of $TBAPW_{11}Re$, the latter cycle (Re^{IV}/Re^{VI}) is quite unlikely as the ^{31}P NMR spectrum of $TBAPW_{11}Re$ after catalytic test (performed with a high excess of reductant) was identical to the freshly prepared $TBAPW_{11}Re^{V}$. Additionally, $TBAPW_{11}Re^{IV}$ is reported to be unstable (it is rapidly

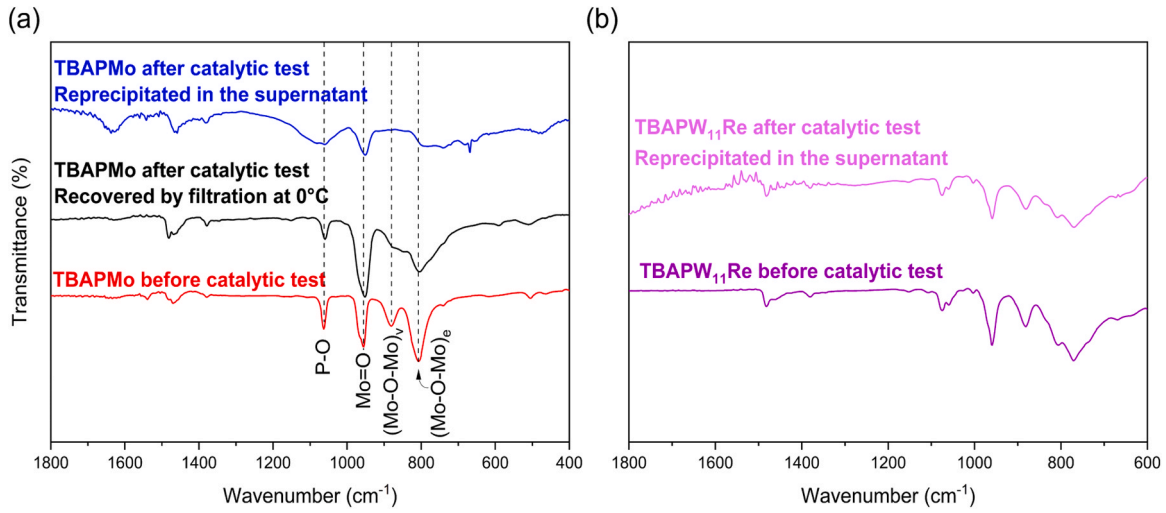

Fig. 12. IR spectra of (a) freshly prepared TBAPMo (before catalytic test), TBAPMo after catalytic test recovered by filtration at 0°C and TBAPMo recovered in the filtrate collected at 90°C; (b) fresh $TBAPW_{11}Re$ and $TBAPW_{11}Re$ recovered in the filtrate collected at 90°C.

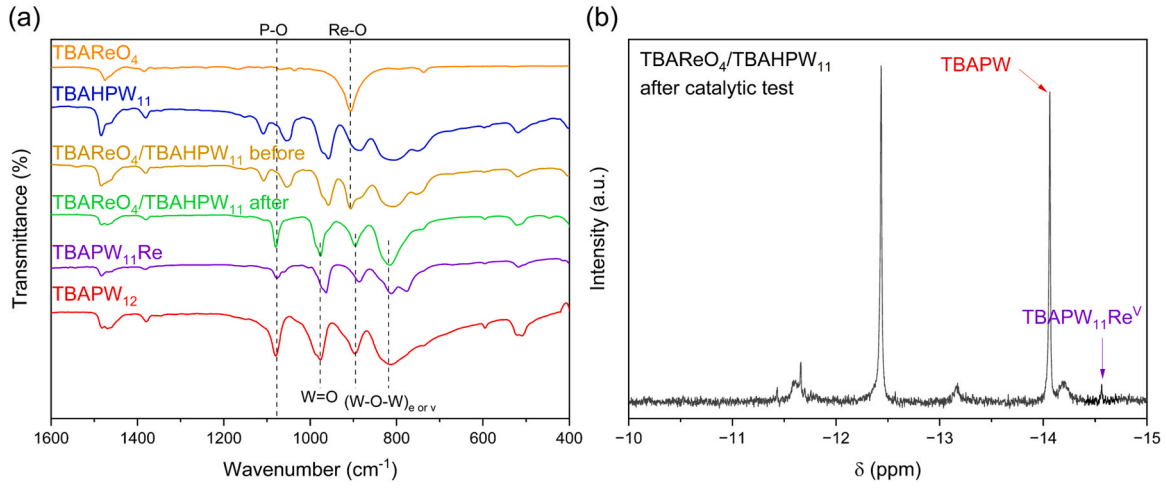

Fig. 13. (a) IR spectra of $TBAReO_4$, $TBAHPW_{11}$, $TBAReO_4/TBAHPW_{11}$ before and after catalytic test, $TBAPW_{11}Re$ and $TBAPW_{12}$. (b) ^{31}P NMR spectrum of $TBAReO_4/TBAHPW_{11}$ after catalytic test. (Note: it presents a contamination peak at −12.45 ppm from the capillary tube used for these analyses.).

oxidized by air) [32]. Thus, assuming a Re^{V}/Re^{VII} mechanism, $TBAPW_{11}Re^{VII}$ could be temporarily decomposed into ReO_4^- and $PW_{11}O_{39}^{7-}$ (PW_{11}). In that case, ReO_4^- could then be the active species and would be able, once reduced into a Re(V) species, to refill the lacuna of PW_{11}. To test the ability of this Re(V) species to refill the PW_{11} lacuna during the catalytic test, a catalytic test was performed with $TBAReO_4/TBAHPW_{11}$ (*viz.* $TBAReO_4$ simply adsorbed at the surface of a $TBAHPW_{11}$ powder) and the remaining solid was analyzed by ^{31}P NMR and IR afterwards to check for the presence of $TBAPW_{11}Re$ (Fig. 13).

The IR spectrum of $TBAReO_4/TBAHPW_{11}$ before catalytic test (Fig. 13 (a)) showed the peaks of both $TBAReO_4$ (Re-O vibration at 909 cm^{-1}) and $TBAHPW_{11}$ (see Fig. 4 (b)), meaning that none of them were altered during the impregnation procedure to adsorb $TBAReO_4$ on $TBAHPW_{11}$. These results are in line with the fact that perrhenates are not able to fill the lacuna of PW_{11}, as reported elsewhere [56]. After catalytic test, the IR spectrum of $TBAReO_4/TBAHPW_{11}$ was identical to $TBAPW_{12}$, hence not showing any presence of $TBAPW_{11}Re$. Still, as the powder showed a slight purple tint (Figure S11), the presence of small amounts of $TBAPW_{11}Re^{V}$ (which is dark-purple) was suspected. Indeed, the ^{31}P NMR of $TBAReO_4/TBAHPW_{11}$ evidenced its presence, but in tiny amounts (Fig. 13 (b)). Additionally, no peak of $TBAHPW_{11}$ could be observed. Instead, the spectrum presented an intense peak of $TBAPW_{12}$.

Table 1
Catalytic performances (hexene yields) of AHM, TBAPMo, $TBAReO_4$, $TBAPW_{11}Re$, Na_2WO_4 and TBAPW. Conditions: 210°C, 18 h, 2 % mol. Re (in the case of $TBAPW_{11}Re$ and $TBAReO_4$), 5 % mol. Mo (in the case of TBAPMo or AHM) or 5 % W (in the case of TBAPW or Na_2WO_4) with respect to the diol. Conversion reached 100 % for all except TBAPW (42 %) and Na_2WO_4 (37 %).

Catalyst	Yield (%)
AHM	48
TBAPMo	55
$TBAReO_4$	99
$TBAPW_{11}Re$	73
Na_2WO_4	3
TBAPW	9

These data demonstrate that the mechanism whereby $TBAPW_{11}Re$ is temporarily unbundled can be excluded, as the presence of $TBAPW_{12}$ after catalytic test with the synthesized $TBAPW_{11}Re$ would then have been evidenced also by ^{31}P NMR, and it is not the case.

The catalytic performances of TBAPMo, $TBAPW_{11}Re$ and TBAPW

were compared with ammonium heptamolybdate (AHM, $(NH_4)_6Mo_7O_{24}$), $TBAReO_4$ and Na_2WO_4, respectively. While TBAPMo showed slightly better catalytic performance than AHM, $TBAReO_4$ converted 1,2-hexanediol with a higher selectivity than $TBAPW_{11}Re$, and Na_2WO_4 was less active than TBAPW (Table 1). However, these catalytic tests are not strictly comparable as only part of the TBAPMo or $TBAPW_{11}Re$ is thought to carry out the reaction, i.e. the part that is dissolved. In those cases, they act as reservoirs of dissolved highly active species. Catalytic tests were also performed with TBAPMo, TBAPW and $TBAPW_{11}Re$ on the biomass-derived 1,4-anhydroerythritol and similar catalytic performances were obtained as with 1,2-hexanediol (Table S1). Hence, the catalytic performances of TBAPMo and $TBAPW_{11}Re$ are promising and are paving the way for the implementation of new Keggin POMs-based catalysts for DODH.

5. Conclusion

We reported the use of Keggin phosphometalates as deoxydehydration catalysts. Tetrabutylammonium (TBA) phosphometalates (M = Mo or W) outperformed NH_4PMs and HPMs, likely due to their non-acidic nature. TBAPMo showed good catalytic performance (yield of 52 %) in the DODH model reaction of 1,2-hexanediol using 3-octanol as both solvent and reductant. While TBAPW showed poor conversion and selectivity (45 % and 20 %, respectively), by contrast, its Re-substituted counterpart ($TBAPW_{11}Re$) displayed excellent performance (100 % conversion, 73 % selectivity) in the same reaction conditions. Investigations via cold filtration and recyclability tests on the nature of the catalytically active species revealed that it is the dissolution of TBAPMo and $TBAPW_{11}Re$ that leads to active homogeneous catalysts, whereas the recyclable solids serve as reservoirs of soluble active species from one run to another. More precisely, IR and ^{31}P NMR experiments showed that the active species are undamaged PMo_{12} and $PW_{11}Re$ polyoxometalates. Notably, this work represents the first study only dedicated to Keggin polyoxometalates as a versatile platform for the elaboration of performant deoxydehydration catalysts. Future works will entail exploring new POM formulations and optimizing their recovery and reuse.

Declaration of Competing Interest

The authors declare that they have no known competing financial interests or personal relationships that could have appeared to influence the work reported in this paper.

Acknowledgements

The first author thanks the Université catholique de Louvain (UCLouvain) for the teaching assistant position at the Bioscience Engineering Faculty. Sarah Eeckhout is acknowledged for her help in the synthesis of the rhenium precursor, $TBAReOCl_4$. Fabio Lucaccioni is acknowledged for the ICP-AES and the elemental analyses. Many thanks to Michaël Scarito for the graphical abstract and the Keggin heteropolyanion scheme elaboration.

Appendix A. Supporting information

Supplementary data associated with this article can be found in the online version at doi:10.1016/j.apcatb.2025.125432.

Data availability

Data will be made available on request.

References

[1] J.R. Dethlefsen, D. Lupp, B.-C. Oh, P. Fristrup, Molybdenum-catalyzed deoxydehydration of vicinal diols, ChemSusChem 7 (2) (2014) 425–428, https://doi.org/10.1002/cssc.201300945.
[2] N.N. Tshibalonza, J.-C.M. Monbaliu, The deoxydehydration (DODH) reaction: a versatile technology for accessing olefins from bio-based polyols, Green. Chem. 22 (15) (2020) 4801–4848, https://doi.org/10.1039/D0GC00689K.
[3] S. Carlier, J. Gripekoven, M. Philippo, S. Hermans, Ru on N-doped carbon supports for the direct hydrogenation of cellobiose into sorbitol, Appl. Catal. B: Environ. 282 (2021) 119515, https://doi.org/10.1016/j.apcatb.2020.119515.
[4] F. Brienza, K. Van Aelst, K. Thielemans, B.F. Sels, D.P. Debecker, I. Cybulska, Enhancing lignin depolymerization via a dithionite-assisted organosolv fractionation of birch sawdust, Green. Chem. 23 (9) (2021) 3268–3276, https://doi.org/10.1039/D1GC00503K.
[5] N. Ota, M. Tamura, Y. Nakagawa, K. Okumura, K. Tomishige, Hydrodeoxygenation of vicinal OH groups over heterogeneous rhenium catalyst promoted by palladium and ceria support, Angew. Chem. 127 (6) (2015) 1917–1920, https://doi.org/10.1002/ange.201410352.
[6] J.H. Jang, H. Sohn, J. Camacho-Bunquin, D. Yang, C.Y. Park, M. Delferro, M. M. Abu-Omar, Deoxydehydration of biomass-derived polyols with a reusable unsupported rhenium nanoparticles catalyst, ACS Sustain. Chem. Eng. 7 (13) (2019) 11438–11447, https://doi.org/10.1021/acssuschemeng.9b01253.
[7] F.C. Jentoft, Transition metal-catalyzed deoxydehydration: missing pieces of the puzzle, Catal. Sci. Technol. (2022), https://doi.org/10.1039/D1CY02083H.
[8] S. Tazawa, N. Ota, M. Tamura, Y. Nakagawa, K. Okumura, K. Tomishige, Deoxydehydration with molecular hydrogen over ceria-supported rhenium catalyst with gold promoter, ACS Catal. 6 (10) (2016) 6393–6397, https://doi.org/10.1021/acscatal.6b01864.
[9] X. Li, D. Wu, T. Lu, G. Yi, H. Su, Y. Zhang, Highly efficient chemical process to convert mucic acid into adipic acid and DFT studies of the mechanism of the rhenium-catalyzed deoxydehydration, Angew. Chem. Int. Ed. 53 (16) (2014) 4200–4204, https://doi.org/10.1002/anie.201310991.
[10] G.K. Cook, M.A. Andrews, Toward nonoxidative routes to oxygenated organics: stereospecific deoxydehydration of diols and polyols to alkenes and allylic alcohols catalyzed by the metal oxo complex $(C_5Me_5)ReO_3$, J. Am. Chem. Soc. 118 (39) (1996) 9448–9449, https://doi.org/10.1021/ja9620604.
[11] L. Sandbrink, E. Klindtworth, H.-U. Islam, A.M. Beale, R. Palkovits, ReO_x/TiO_2: a recyclable solid catalyst for deoxydehydration, ACS Catal. 6 (2) (2016) 677–680, https://doi.org/10.1021/acscatal.5b01936.
[12] B.E. Sharkey, A.L. Denning, F.C. Jentoft, R. Gangadhara, T.V. Gopaladasu, K. M. Nicholas, New solid oxo-rhenium and oxo-molybdenum catalysts for the deoxydehydration of glycols to olefins, Catal. Today 310 (2018) 86–93, https://doi.org/10.1016/j.cattod.2017.05.090.
[13] L. Sandbrink, K. Beckerle, I. Meiners, R. Liffmann, K. Rahimi, J. Okuda, R. Palkovits, Supported molybdenum catalysts for the deoxydehydration of 1,4-anhydroerythritol into 2,5-dihydrofuran, ChemSusChem 10 (7) (2017) 1375–1379, https://doi.org/10.1002/cssc.201700010.
[14] G. Chapman, K.M. Nicholas, Vanadium-catalyzed deoxydehydration of glycols, Chem. Commun. 49 (74) (2013) 8199–8201, https://doi.org/10.1039/C3CC44656E.
[15] T.V. Gopaladasu, K.M. Nicholas, Carbon monoxide (CO)- and hydrogen-driven, vanadium-catalyzed deoxydehydration of glycols, ACS Catal. 6 (3) (2016) 1901–1904, https://doi.org/10.1021/acscatal.5b02667.
[16] K.A. DeNike, Catalytic Activity of Tungsten-Dioxo and Tungsten-Diimido Complexes, University of Arkansas, Fayetteville, 2022. ⟨https://scholarworks.uark.edu/etd/4584/⟩ (accessed 2023-01-30).
[17] A.L. Denning, H. Dang, Z. Liu, K.M. Nicholas, F.C. Jentoft, Deoxydehydration of glycols catalyzed by carbon-supported perrhenate, ChemCatChem 5 (12) (2013) 3567–3570, https://doi.org/10.1002/cctc.201300545.
[18] J. Li, M. Lutz, M. Otte, R.J.M.A. KleinGebbink, Cp^{tt}-based trioxo-rhenium catalyst for the deoxydehydration of diols and polyols, ChemCatChem 10 (20) (2018) 4755–4760, https://doi.org/10.1002/cctc.201801151.
[19] Wagner, N.; Tang, W.-C.; Wagner, J.; Nguyen, B.; Lam, J.; Gibbons-Stovall, S.; Matias, A.; Martinez, S.; Trieu-Tran, T.; Clabaugh, G.; Navarro, C.; Abboud, I.; Flores, F.; Nicholas, K.; John, A. Molybdenum Catalysts Based on Salan Ligands for the Deoxydehydration Reaction. March 29, 2024. https://doi.org/10.26434/chemrxiv-2024-k94kx.
[20] Tomishige, K. Deoxydehydration of Methyl Glycosides with Cis-Vicinal OH Groups Using ReO_x/CeO_2 Catalysts Modified with Metallic Particles and H_2 Reductant, 2022.
[21] X. Geng, M. Xu, C. Yang, J. Zhang, Z. Fang, R. Sun, K. Guo, Recent progress on non-noble metal catalysts for the deoxydehydration of biomass-derived oxygenates, Green. Process. Synth. 12 (2023), https://doi.org/10.1515/gps-2023-0129.
[22] A.R. Petersen, P. Fristrup, New motifs in deoxydehydration: beyond the realms of rhenium, Chem. – A Eur. J. 23 (43) (2017) 10235–10243, https://doi.org/10.1002/chem.201701153.
[23] J. Díaz, L.R. Pizzio, G. Pecchi, C.H. Campos, L. Azócar, R. Briones, R. Romero, A. Henríquez, E.M. Gaigneaux, D. Contreras, Tetrabutyl ammonium salts of keggin-type vanadium-substituted phosphomolybdates and phosphotungstates for selective aerobic catalytic oxidation of benzyl alcohol, Catalysts 12 (5) (2022), https://doi.org/10.3390/catal12050507.
[24] G. Hidalgo, G. Barozzino-Consiglio, M. Devillers, E.M. Gaigneaux, Active epoxidation bipyridine-oxodiperoxotungstate catalysts, Mol. Catal. 528 (2022) 112479, https://doi.org/10.1016/j.mcat.2022.112479.

[25] C. Lang, J. Schnee, B.J. Takam Mba, F. Devred, E.M. Gaigneaux, Ammonium-substitution for successfully activating the bulk of keggin acid salts in 1-butanol dehydration, Catal. Sci. Technol. 10 (18) (2020) 6244–6256, https://doi.org/10.1039/D0CY00820F.

[26] J. Schnee, A. Eggermont, E.M. Gaigneaux, Boron nitride: a support for highly active heteropolyacids in the methanol-to-DME reaction, ACS Catal. 7 (6) (2017) 4011–4017, https://doi.org/10.1021/acscatal.7b00808.

[27] J. Schnee, E.M. Gaigneaux, Elucidating and exploiting the chemistry of keggin heteropolyacids in the methanol-to-DME conversion: enabling the bulk reaction thanks to operando Raman, Catal. Sci. Technol. 7 (4) (2017) 817–830, https://doi.org/10.1039/C6CY02264B.

[28] J. Song, Z. Luo, H. Zhu, Z. Huang, T. Lian, A.L. Kaledin, D.G. Musaev, S. Lense, K. I. Hardcastle, C.L. Hill, Synthesis, structure, and characterization of two polyoxometalate–photosensitizer hybrid materials, Inorg. Chim. Acta 363 (15) (2010) 4381–4386, https://doi.org/10.1016/j.ica.2010.07.022.

[29] Jan-Christian Raabe, José Aceituno Cruz, A. Jakob, M.J. Poller, Comparative spectroscopic and electrochemical study of V(V)-substituted keggin-type phosphomolybdates and -tungstates, Inorganics 11 (4) (2023) 138, https://doi.org/10.3390/inorganics11040138.

[30] Dilworth, J.R.; Hussain, W.; Hutson, A.J.; Jones, C.J.; Mcquillan, F.S.; Mayer, J.M.; Arterburn, J.B. Tetrahalo Oxorhenate Anions. In *Inorganic Syntheses*; Inorganic Syntheses; 1996; pp 257–262. https://doi.org/10.1002/9780470132623.ch42.

[31] Karcher, J. Functionalized Polyoxometalates for Advanced Applications, Manhattan, 2007. ⟨http://hdl.handle.net/2097/273⟩ (accessed 2023-09-01).

[32] F. Ortega, M.T. Pope, Polyoxotungstate anions containing high-valent rhenium. 1. Keggin anion derivatives, Inorg. Chem. 23 (21) (1984) 3292–3297, https://doi.org/10.1021/ic00189a005.

[33] K.A. DeNike, S.M. Kilyanek, Deoxydehydration of vicinal diols by homogeneous catalysts: a mechanistic overview, R. Soc. Open Sci. 6 (11) (2019) 191165, https://doi.org/10.1098/rsos.191165.

[34] P.M. Słomkiewicz, Isomerization of linear alkenes on amberlyst 15, Appl. Catal. A: Gen. 301 (2) (2006) 232–240, https://doi.org/10.1016/j.apcata.2005.12.012.

[35] W. Ma, L. Zhang, D. Wang, J. Zhao, B. Liu, L. Zhang, Catalytic isomerization of olefins and their derivatives: a brief overview, in: R. Davarnejad (Ed.), Alkenes - Recent Advances, New Perspectives and Applications, IntechOpen, Rijeka, 2021, https://doi.org/10.5772/intechopen.99076.

[36] J.J. Altenau, M.T. Pope, R.A. Prados, Hyunsoo So, Models for heteropoly blues. degrees of valence trapping in vanadium(IV)- and molybdenum(V)-substituted keggin anions, Inorg. Chem. 14 (2) (1975) 417–421, https://doi.org/10.1021/ic50144a042.

[37] M.T. Pope, Introduction to Polyoxometalate Chemistry, in: J.J. Borrás-Almenar, E. Coronado, A. Müller, M. Pope (Eds.), Polyoxometalate Molecular Science, Springer Netherlands, Dordrecht, 2003, pp. 3–31, https://doi.org/10.1007/978-94-010-0091-8_1.

[38] C. Dablemont, A. Proust, R. Thouvenot, C. Afonso, F. Fournier, J.-C. Tabet, Functionalization of polyoxometalates: from lindqvist to Keggin derivatives. 1. synthesis, solution studies, and spectroscopic and ESI mass spectrometry characterization of the rhenium phenylimido tungstophosphate $[PW_{11}O_{39}\{ReNC_6H_5\}]_4$, Inorg. Chem. 43 (11) (2004) 3514–3520, https://doi.org/10.1021/ic0499042.

[39] C.N. Kato, K. Hara, M. Kato, H. Amano, K. Sato, Y. Kataoka, W. Mori, EDTA-reduction of water to molecular hydrogen catalyzed by visible-light-response TiO_2-based materials sensitized by Dawson- and Keggin-Type Rhenium(V)-containing polyoxotungstates, Materials 3 (2) (2010) 897–917, https://doi.org/10.3390/ma3020897.

[40] A. Besserguenev, M.T. Pope, Salts of a Sandwich-Type Bis 9-Tungstoarsenate(III) Tris(Oxorhenate(V)) Polyoxoanion as Precursors to Tungsten–Rhenium Bronzes, Comptes Rendus Chim. 8 (6) (2005) 933–955, https://doi.org/10.1016/j.crci.2004.10.005.

[41] C. Dablemont, A. Proust, R. Thouvenot, C. Afonso, F. Fournier, J.-C. Tabet, Investigation of the Reactivity of Arylamines, Organo-Hydrazines and Tolylisocyanate towards $[PW_{12-x}M_xO_{40}]^{N-}$ Keggin Anions, Dalton Trans. (10) (2005) 1831–1841, https://doi.org/10.1039/B500270B.

[42] C. Dablemont, C.G. Hamaker, R. Thouvenot, Z. Sojka, M. Che, E.A. Maatta, A. Proust, Cover picture: functionalization of heteropolyanions—osmium and rhenium nitrido derivatives of Keggin- and Dawson-Type polyoxotungstates: synthesis, characterization and multinuclear (^{183}W, ^{15}N) NMR, EPR, IR, and UV/Vis Fingerprints, Chem. – A Eur. J. 12 (36) (2006), https://doi.org/10.1002/chem.200690114, 9111–9111.

[43] D.C. Batalha, S.O. Ferreira, R.C. da Silva, M.J. da Silva, Cesium-exchanged lacunar keggin heteropolyacid salts: efficient solid catalysts for the green oxidation of terpenic alcohols with hydrogen peroxide, ChemistrySelect 5 (6) (2020) 1976–1986, https://doi.org/10.1002/slct.201903437.

[44] P.T. Meiklejohn, M.T. Pope, R.A. Prados, Synthesis of heteropoly anions in aprotic solvents. Tungstorhenates(V),-(VI), and -(VII), J. Am. Chem. Soc. 96 (21) (1974) 6779–6781, https://doi.org/10.1021/ja00828a051.

[45] L.A. Combs-Walker, C.L. Hill, Stabilization of the defect ("lacunary") complex polymolybdophosphate, $PMo_{11}O_{39}^{7-}$. Isolation, purification, stability characteristics, and metalation chemistry, Inorg. Chem. 30 (21) (1991) 4016–4026, https://doi.org/10.1021/ic00021a010.

[46] M. Fournier, C. Rocchiccioli-Deltcheff, L.P. Kazansky, Infrared spectroscopic evidence of bipolaron delocalization in reduced heterododecamolybdates, Chem. Phys. Lett. 223 (4) (1994) 297–300, https://doi.org/10.1016/0009-2614(94)00454-4.

[47] J.C. Védrine, J.-M.M. Millet, Heteropolyoxometallate catalysts for partial oxidation, Met. Oxide Catal. (2008) 561–594, https://doi.org/10.1002/9783527626113.ch14.

[48] E.A. Nagul, I.D. McKelvie, P. Worsfold, S.D. Kolev, The molybdenum blue reaction for the determination of orthophosphate revisited: opening the black box, Anal. Chim. Acta 890 (2015) 60–82, https://doi.org/10.1016/j.aca.2015.07.030.

[49] K.A. Phipps, Redox Chemistry of Polyoxometalates and Applications in Energy Storage, Newcastle University, Newcastle, 2020. ⟨http://theses.ncl.ac.uk/jspui/handle/10443/5162⟩ (accessed 2023-09-05).

[50] R.I. Maksimovskaya, Molybdophosphate heteropoly blues: electron-transfer reactions in aqueous solutions as studied by NMR, Polyhedron 65 (2013) 54–59, https://doi.org/10.1016/j.poly.2013.08.014.

[51] J.F. Garvey, M.T. Pope, Chirality of oxidized and reduced octadecamolybdodiphosphate anions. Observation of a pfeiffer effect, Inorg. Chem. 17 (5) (1978) 1115–1118, https://doi.org/10.1021/ic50183a004.

[52] M. Pascual-Borràs, E. Arca, H. Yoshikawa, T. Penfold, P.G. Waddell, R.J. Errington, Mechanochemical polyoxometalate super-reduction with lithium metal, J. Am. Chem. Soc. 146 (38) (2024) 26485–26496, https://doi.org/10.1021/jacs.4c09998.

[53] H.-R. Sun, S.-Y. Zhang, J.-Q. Xu, G.-Y. Yang, T.-S. Shi, Electrochemical and in-situ UV-visible-near-IR and FTIR spectroelectrochemical characterisation of the mixed-valence heteropolyanion $PMo_{12}O_{40}^{n-}$ (N=4, 5, 6, 7) in aprotic media, J. Electroanal. Chem. 455 (1) (1998) 57–68, https://doi.org/10.1016/S0022-0728(98)00150-8.

[54] N. Mizuno, K. Katamura, Y. Yoneda, M. Misono, Catalysis by heteropoly compounds: V. The reduction mechanism of H3PMo12O40, J. Catal. 83 (2) (1983) 384–392, https://doi.org/10.1016/0021-9517(83)90063-5.

[55] R. Hosaka, D. Asada, J. Cao, M. Tamura, Y. Nakagawa, K. Tomishige, J. Hasegawa, A. Nakayama, Reaction mechanism of deoxydehydration by ceria-supported monomeric rhenium catalysts: a computational study, J. Phys. Chem. C 126 (28) (2022) 11566–11573, https://doi.org/10.1021/acs.jpcc.2c02944.

[56] B. Charreton, R. Meunier, Réaction de l'ion chlororhénate(IV) avec différents polyanions tungstiques, R. Acad. Sci. Paris (1972) 945–948.